

AD A045585

BRL MR 2788

BRL

AD

MEMORANDUM REPORT NO. 2788

(Supersedes IMR No. 477)

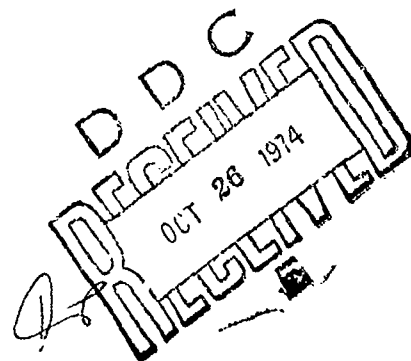
SPALL RING DIAMETER AND PATHS OF
PERIPHERAL SPALL PARTICLES FROM SHAPED
CHARGE JET PERFORATION OF ARMOR PLATE

Eugene T. Roecker

September 1977

Approved for public release; distribution unlimited.

USA ARMAMENT RESEARCH AND DEVELOPMENT COMMAND
USA BALLISTIC RESEARCH LABORATORY
ABERDEEN PROVING GROUND, MARYLAND



AD No. _____
DDC FILE COPY

Destroy this report when it is no longer needed.
Do not return it to the originator.

Secondary distribution of this report by originating
or sponsoring activity is prohibited.

Additional copies of this report may be obtained
from the National Technical Information Service,
U.S. Department of Commerce, Springfield, Virginia
22151.

The findings in this report are not to be construed as
an official Department of the Army position, unless
so designated by other authorized documents.

*The use of trade names or manufacturers' names in this report
does not constitute indorsement of any commercial product.*

UNCLASSIFIED

SECURITY CLASSIFICATION OF THIS PAGE (When Data Entered)

14 BRL-MR-2788

REPORT DOCUMENTATION PAGE		READ INSTRUCTIONS BEFORE COMPLETING FORM
1. REPORT NUMBER BRL MEMORANDUM REPORT NO. 2788	2. GOVT ACCESSION NO.	3. RECIPIENT'S CATALOG NUMBER
4. TITLE (and Subtitle) SPALL RING DIAMETER AND PATHS OF PERIPHERAL SPALL PARTICLES FROM SHAPED CHARGE JET PERFORATION OF ARMOR PLATE	5. TYPE OF REPORT & PERIOD COVERED 9 Final rept.	
7. AUTHOR(s) Eugene T. Roecker	6. PERFORMING-ORG. REPORT NUMBER	
9. PERFORMING ORGANIZATION NAME AND ADDRESS USA Ballistic Research Laboratory Boerdeen Proving Ground, MD 21005	8. CONTRACT OR GRANT NUMBER(s)	
11. CONTROLLING OFFICE NAME AND ADDRESS US Army Materials & Mechanics Research Center Watertown, MA 02172	10. PROGRAM ELEMENT, PROJECT, TASK AREA & WORK UNIT NUMBERS 16 17 1E762708A090418	
14. MONITORING AGENCY NAME & ADDRESS (if different from Controlling Office)	12. REPORT DATE SEP 1977	
	13. NUMBER OF PAGES 25 12, 23p.	
	15. SECURITY CLASS. (of this report) UNCLASSIFIED	
16. DISTRIBUTION STATEMENT (of this Report) Approved for public release; distribution unlimited.	15a. DECLASSIFICATION/DOWNGRADING SCHEDULE	
17. DISTRIBUTION STATEMENT (of the abstract entered in Block 20, if different from Report)		
18. SUPPLEMENTARY NOTES This memorandum report supersedes interim memorandum report 477, February 1976.		
19. KEY WORDS (Continue on reverse side if necessary and identify by block number) Spall Ring Shaped Charge Jet Armor Perforation Super Spall		
20. ABSTRACT (Continue on reverse side if necessary and identify by block number) The 3.2-inch BRL precision shaped charge warhead was statically fired into armor plate of foreign and domestic production. The standoff distances varied from 2 to 12 cone diameters; the plate thicknesses, from 2 to 30 centimeters; and the Brinell hardness numbers of the armor from 100 to 450. Measurements of the diameter of the resulting spall scab on the back surface of the target correlate well with the rate of transfer of energy from jet to target. Analysis suggests that "super spall" may be produced by nearness of the		

DDC
OCT 26 1974
REGISTERED

UNCLASSIFIED

SECURITY CLASSIFICATION OF THIS PAGE(When Data Entered)

20. ABSTRACT (CONTINUED)

→ fatter, leading portion of the jet to the back surface of thin plates.
Some meager information on the trajectories of peripheral spall particles
is also presented. ↑

2

UNCLASSIFIED

SECURITY CLASSIFICATION OF THIS PAGE(When Data Entered)

TABLE OF CONTENTS

	<u>Page</u>
1. INTRODUCTION	5
2. EXPERIMENT	5
3. THE PARAMETERS OF THE EXPERIMENT	7
3.1 Why jet characteristics instead of warhead parameters?	7
3.2 Shaped charge jet in flight	7
3.3 Resulting penetrator-target parameters	12
3.4 Simplification by use of rate of energy transfer. . .	12
4. RESULTS AND DISCUSSION	14
4.1 Diameter of spall scab	14
4.1.1 Targets with BHN from 250 to 450	15
4.1.2 Targets with BHN of 100	15
4.1.3 "Super Spall"	15
4.2 Peripheral Spall Trajectories	18
4.2.1 Target plates of BHN from 250 to 450	19
4.2.2 Target Plates of BHN 100	19
5. CONCLUSIONS	19
DISTRIBUTION LIST	23

ACCESSION FOR	
THIS	Write Section <input checked="" type="checkbox"/>
DOC	Buff Section <input type="checkbox"/>
UNCLASSIFIED	
CLASSIFICATION	
DISTRIBUTION/AVAILABILITY CODES	
or SPECIAL	

1. INTRODUCTION

To determine the vulnerability of military targets protected by armor, one must assess the interior damage resulting from spall off the back surface of such armor as well as the damage caused by the residual penetrator and by the target-penetrator ejecta. (Ejecta spewed in front of the armor is ignored.) The Ballistic Research Laboratory (BRL) is building a data bank to provide such an assessment for spall and ejecta* produced by the shaped charge jet penetration of steel armor plate.

A characterization of debris (spall plus ejecta) was made by Systems, Science, and Software, Incorporated (S³) under BRL contract¹. In reviewing the S³ effort, it was decided that data associated with the periphery of the spall scab could be correlated with penetration parameters. This report presents the result of such a correlation.

2. EXPERIMENT

The details of the experimental set-up can be found in References 2 and 3. A schematic of the firings is shown in Figure 1.

¹R. T. Sedgwick, et al, "Characterization of Behind-the-Armor Debris Resulting from Shaped Charge Jet Formation," (sic), Systems, Science, and Software, Incorporated, Ballistic Research Laboratory Contract Report No. 249, July 1975 (AD #B006721L).

²Barry H. Rodin, "Documentation of Spall Produced by a 2.3 Inch Precision Shaped Charge," Ballistic Research Laboratory Memorandum Report No. 2407, August 1974 (AD #923573L).

³C. J. Brown and R. Karpp, "Comparative Effectiveness of Foreign and Domestic Armors Against Shaped Charge Attack," Ballistic Research Laboratory Report No. 1902, August 1976. (AD #B013219L)

*The author interprets spall to mean material released from the armor because of the tensile wave reflected from the back surface, often called scabbing to distinguish from front surface spall. Target material, along with penetrator material, that is residue of the penetration process and that is pushed out by the remaining penetrator is thought of as ejecta.

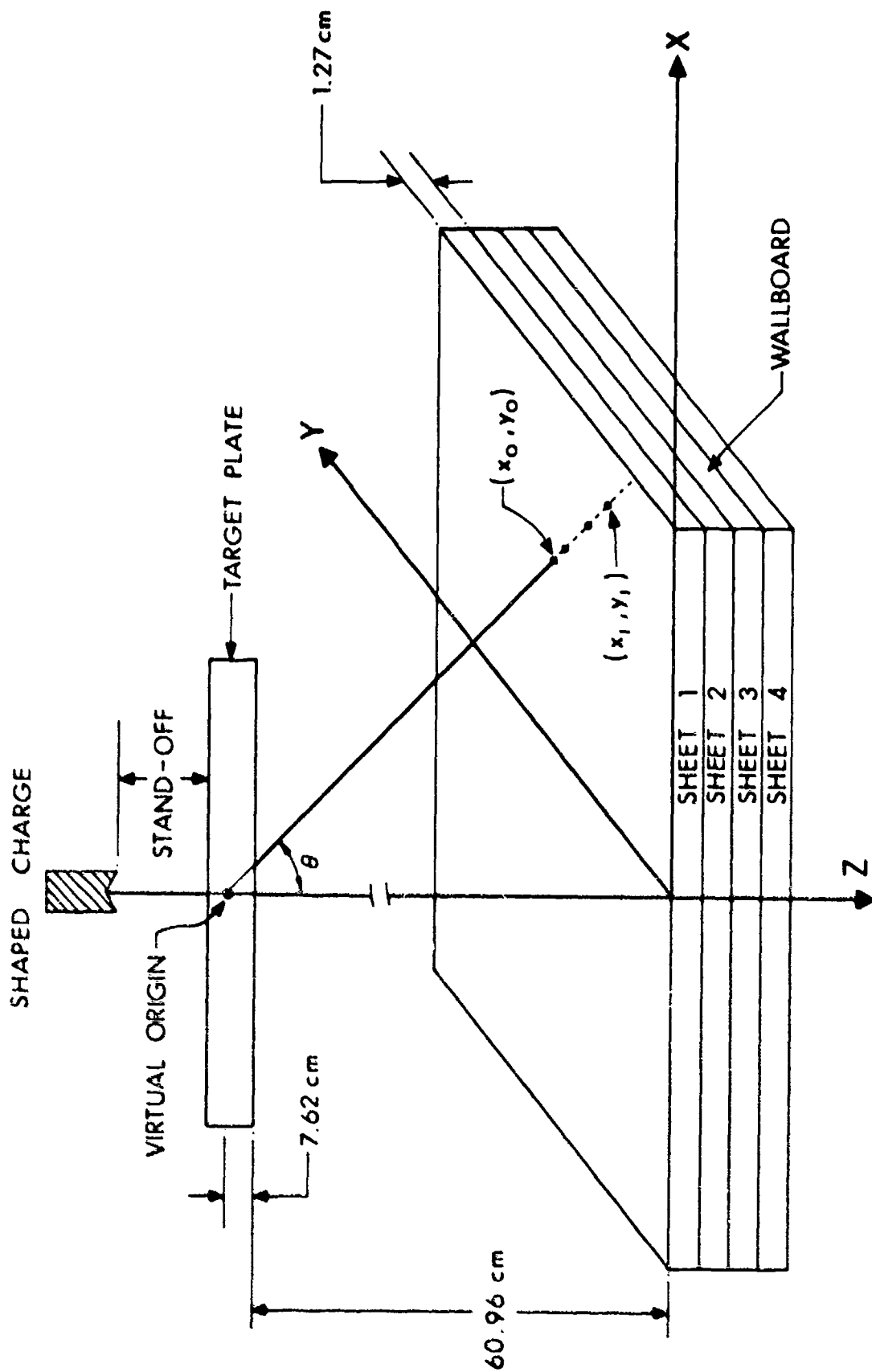


FIGURE 1. Schematic Diagram of Test Setup.

The shaped charge used was the 3.2-in. BRL precision copper liner loaded with Composition B explosive. A description of the relationship between jet penetration and jet characteristics can be found in Reference 4. The jet in this experiment has the following measured characteristics:

- . Virtual origin is 7.5 cm uprange of the base of the liner.
- . Velocity of the tip of the jet is 7.8 km/s.
- . Breakup time is 115 microsec.
- . Length of leading pellet after breakup time is 3.2 cm.
- . Diameter of leading pellet after breakup time is 0.4 cm.
- . Diameter of main jet after breakup time is 0.2 cm.

The standoff distance varied from two to twelve cone diameters. The target plate thicknesses varied from 2.22 cm (7/8 inch) to 30.48 cm (12 inches). The hardness of the armor varied from a Brinell hardness number (BHN) of 100 to 450 with the armor being of both foreign and domestic production. Some analysis of the foreign and domestic armor data was also done by Brown and Karpp³. Table 1 lists the standoff, target thickness, and target properties for each round. (The above jet characteristics are assumed the same for each round.)

3. THE PARAMETERS OF THE EXPERIMENT

3.1 Why Jet Characteristics Instead of Warhead Parameters?

Since one objective is to provide spall release criteria for hydro-code simulation, we choose to correlate target effects (spall) with parameters available during such simulation, namely, parameters describing the on-going penetration process. Warhead parameters, so popular for characterizing target effects for vulnerability calculations, do not fulfill this request since they do not lend themselves to correlation with the dynamic history of the penetration process. When the warhead is a shaped charge, however, the associated jet characteristics provide parameters quite amenable to such correlation. And, where vulnerability calculations still require "curves" showing target effects vs warhead parameters, they can be inferred from the jet characteristics.

3.2 Shaped Charge Jet in Flight.

All elements of the jet can be visualized as emanating from a single point in space on the axis of the conical liner at the same instant in

⁴ R. Di Persio, et al, "Characteristics of Jets from Small Caliber Shaped Charges with Copper and Aluminum Liners," Ballistic Research Laboratories Memorandum Report No. 1866, September 1967. (AD #823839)

Table 1. Spall Ring Diameter and Path Angle

Target Thickness (cm)	Standoff Distance (C.D.)	dE/dt <u>joules</u> nanosec	BHN	Round No.	Spall Ring Diameter (cm)	Peripheral Spall Path Angle (deg)		
2.2	2	9.5	260**	1166	5.7	45.6		
			260**	67	5.7	47.5		
			260**	68	5.7	42.7		
	12	11.2*	260**	69	5.7	44.1		
			260**	70	5.7	44.7		
			260**	71	5.7	43.3		
2.5	2	9.0	260	96	5.7	48.4		
			260	97	5.7	42.9		
			260	98	5.7	39.9		
			350	1084	5.7	40.2		
			350	85	5.7	48.9		
	5	20.4*	350	86	5.7	47.7		
			350	87	5.7	43.5		
			350	88	5.7	46.0		
			8	14.4*	350	89	5.7	44.7
					350	90	5.7	43.2
	350	91			5.7	41.7		
	12	11.2*			350	92	5.7	40.1
					350	93	5.7	44.8
			350	94	5.7	42.0		
			350	95	5.7	42.5		
			260	1199	5.7	43.7		
	260	1200	5.7	41.9				
	260	01	5.7	46.0				
	4.4	2	6.4	440**	1172	5.4	44.4	
				440**	73	5.7	44.9	

TABLE I. Spall Ring Diameter and Path Angle (Continued)

Target Thickness (cm)	Standoff Distance (C.D.)	dE/dt <u>joules</u> nanosec	BHN	Round No.	Spall Ring Diameter (cm)	Peripheral Spall Path Angle (deg)
4.4	2	6.4	440**	1174	5.7	43.6
			450	78	6.4	41.6
			450	79	6.4	46.1
			450	80	6.4	40.8
	12	***	450	81	5.1	44.5
			450	82	5.1	42.2
			450	83	6.4	40.9
			440**	75	4.1	45.3
			440**	76	3.2	38.4
			440**	77	5.1	40.3
7.6	2	3.8	350	1096	4.4	42.2
			350	97	4.4	44.8
			350	98	4.4	36.6
	5	3.2	350	99	3.8	47.6
			350	1100	3.8	50.6
			350	01	3.8	40.8
	8	2.6	350	02	3.2	40.4
			350	03	3.2	37.7
			350	04	3.2	38.4
	12	2.2	350	05	3.2	44.1
			350	06	3.2	34.6
			350	07	3.8	44.0
9.8	2	2.7	270**	90	4.4	45.4
			270**	91	4.4	43.1
			270**	92	4.4	43.5
	12	2.0	270**	93	3.8	2.0

TABLE I. Spall Ring Diameter and Path Angle (Continued)

Target Thickness (cm)	Standoff Distance (C.D.)	dE/dt		Round No.	Spall Ring Diameter (cm)	Peripheral Spall Path Angle (deg)
		$\frac{\text{joules}}{\text{nanosec}}$	BHN			
9.8	12	2.0	270**	1194	3.2	30.2
			270**	95	3.8	34.3
10.2	2	2.6	270	84	4.4	38.6
			270	85	4.4	47.5
			270	86	4.4	40.7
	12	2.0	270	87	2.5	30.2
			270	88	3.5	34.5
			270	89	3.2	45.4
15.2	2	1.3	350	08	3.5	43.4
			350	09	3.5	36.5
			350	10	3.5	40.2
			350	11	3.5	42.7
	5	1.8	350	12	2.9	38.7
			350	13	2.9	42.7
			350	15	2.9	39.2
	8	1.8	350	16	2.5	39.3
			350	17	2.5	38.6
			350	18	2.5	32.0
	12	1.6	350	19	2.5	43.9
			350	20	2.5	43.3
			350	21	2.5	32.7
30.5	2	0.28	350	26	1.6	18.6
			350	27	1.6	7.5
	5	0.65	350	28	NO SPALL	
			350	29	1.6	26.9

TABLE I. Spall Ring Diameter and Path Angle (Continued)

Target Thickness (cm)	Standoff Distance (C.D.)	dE/dt <u>joules</u> nanosec	BHN	Round No.	Spall Ring Diameter (cm)	Peripheral Spall Path Angle (deg)
30.5	8	0.76	350	1130	1.9	28.5
			350	31	NO SPALL	
2.5	2	9.0	100	39	7.6	38.4
			100	40	8.9	41.1
			100	41	8.3	41.3
	12	11.2*	100	42	8.3	36.3
			100	43	7.6	44.7
			100	44	7.6	34.3
7.6	2	3.8	100	45	8.9	38.0
			100	46	8.9	38.7
			100	47	NO SPALL	
	12	2.2	100	48	NO SPALL	
			100	49	5.1	31.7
			100	50	3.8	35.9
22.9	2	0.55	100	51	3.2	16.3
			100	52	3.2	32.7
			100	53	3.2	7.4
	12	1.1	100	54	3.8	34.9
			100	55	3.8	28.5
			100	56	3.2	40.1

*Energy is transferred by leading portion of the jet (twice the diameter of the remainder of the jet).

**Foreign armor

***Value uncertain since position in target is near the abrupt change in jet diameter between the leading and trailing portions of the jet. dE/dt lies between 2.6 and 10.4 joules/nanosec. Note large scatter in spall diameter.

time ($t = 0$). Any cross section of the jet at some time t , however, has a different velocity than any other cross section. The velocity decreases linearly with position as one moves to the rear of the jet. We have, therefore, a stretching of the jet with time. Since we may think of the jet material as maintaining uniform density during flight, the elongation of the jet must be accompanied by that shrinking of the diameter that preserves the volume of any element of the jet. This stretching continues until such a time ($t = t_1$) that the jet breaks up into discrete elements as shown in Figure 2. Thereafter, the discrete particles continue in flight, each with its own velocity (mean value at $t = t_1$), no longer elongating. There is, of course, some retardation due to air resistance. This effect has been measured⁵ and could be included in this presentation. The effect on spall is felt to be negligible and is avoided for simplicity.

3.3 Resulting Penetrator-Target Parameters.

Since we are addressing here only steel targets and copper jets, each of uniform material density, we restrict our penetrator-target parameters to penetrator diameter, penetrator velocity, target thickness, and target hardness. (Penetrator length is always sufficient to perforate the target.)

The effect of standoff distance can, therefore, be handled by prescribing the known velocity and diameter of each cross section of the jet at time of impact and at any time during penetration.

The penetration process is clearly described in Reference 5. The theory, well supported by experimental evidence, identifies at any instant of time what portion of the jet remains to do further penetration. The effect of target thickness can, therefore, be handled by permitting this theory to identify what portion of the jet is doing the penetrating at any desired time. The diameter of that portion is calculated according to the description above.

Thus, we are able to calculate the velocity and diameter of the cross section of the jet at the target-penetrator interface for all penetration time; and these jet parameters will be used to supplant two control variables for our experiment, standoff distance and target thickness. The remaining two variables, target hardness and foreign vs domestic production, will be handled by searching for differences in the data.

3.4 Simplification by Use of Rate of Energy Transfer.

Our problem is simplified if we are able to find a functional that maps the velocity and diameter of the jet into a single number that

⁵R. Di Persio, J. Simon, and A. B. Merendino, "Penetration of Shaped-Charge Jets into Metallic Targets," Ballistic Research Laboratories Report No. 1296, September 1965. (AD #476717)

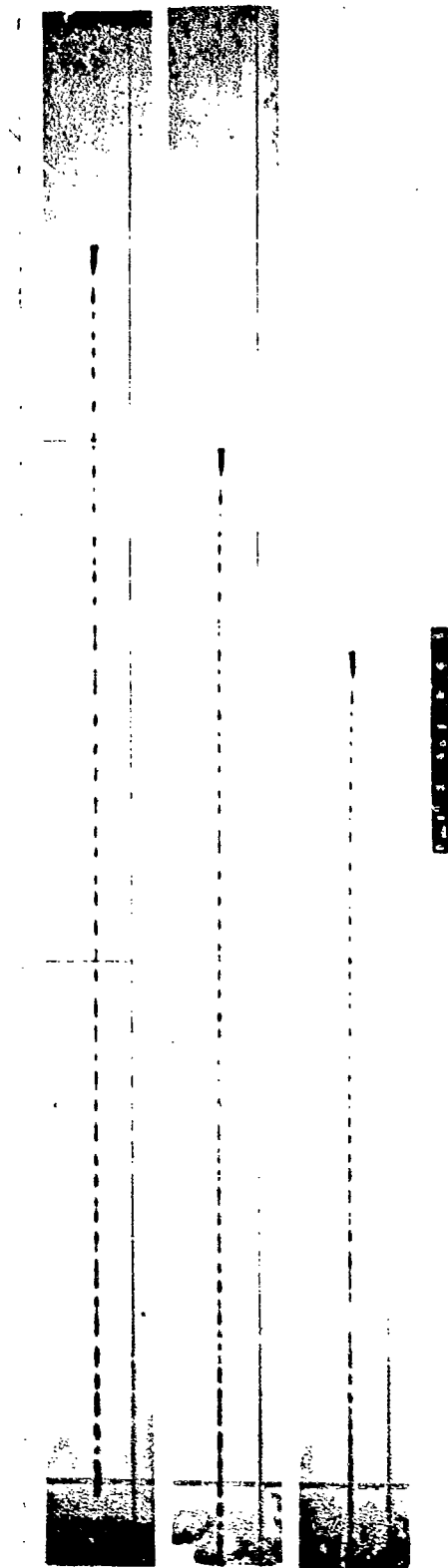


FIGURE 2. Jet of the 3.2 inch Precision Shaped Charge

correlates with the spall measurements. One good candidate for such a functional is the rate at which energy is transferred, dE/dt , from the penetrator to the target when the interface reaches a specific location at or near the back surface of the target. The back surface was the choice of Eichelberger and Regan⁶ and later authors when the number of debris particles was the target response variable. These writers separated the rate of energy transfer into $(dE/dP) \times (dP/dt)$ where P is penetration. Unlike dE/dt these terms can be evaluated without knowing jet diameter per se. The penetration velocity, dP/dt , can be calculated using the ideal jet penetration theory in Reference 5. The term dE/dP is proportional to the cross-sectional area of the penetration hole⁷ and, hence, measurable to within a constant of proportionality.

In keeping with the idea, however, to provide spall release criteria for use in hydrocode simulation, we do not want to correlate spall with any effects (area of hole) that are not known until the event is all over. Therefore, we will deal directly with dE/dt which can be calculated from the known jet characteristics.⁷

In sum, we have reduced the target, warhead, and standoff parameters of the experiment to three: rate of transfer of energy from jet to target, target hardness, and foreign vs domestic armor production.

4. RESULTS AND DISCUSSION

Since other authors^{1,2} have already reported other results from this experiment, we restrict our discussion to spall scab diameter, "superspall," and peripheral spall trajectories.

4.1 Diameter of Spall Scab.

Table 1 lists the measured diameter of the spall ring (scab) for each firing. We desired first to correlate these measurements with the rate of energy transfer at the instant the penetrator-target interface has reached some location near the back surface of the target. After trying a few locations between the back surface and a position 7.5 cm ahead of the back surface, we decided that the best choice was one centimeter ahead of the back surface. The other positions appeared to be only slightly inferior choices.

⁶ J. M. Regan and R. J. Eichelberger, "Prediction of Effectiveness of Shaped Charge Warhead Designs," Ballistic Research Laboratories Technical Note No. 1296, January 1960. (AD #374409)

⁷ A. Merendino, R. Di Persio, and J. Simon, "A Method for Predicting Spallation from Targets Perforated by Shaped Charge Jets," Ballistic Research Laboratories Report No. 1308, January 1966. (AD 371925)

4.1.1 Targets with BHN from 250 to 450. Figure 3 is a plot of the spall diameter from armor plate with BHN of 250 to 450 vs dE/dt, the rate of energy transfer when penetration has reached a position one centimeter ahead of the back surface of the plate. The data seem to correlate well with this parameter. The levels of hardness are symbolized by 2, 3, and 4 for nominal BHN of 240, 350, and 450, respectively. There is no discernible effect due to hardness in this range. Nor are there any clear differences between the foreign and domestic armor. Figure 3 shows the spall diameter increasing linearly (?) with dE/dt from hole diameter at low dE/dt to a diameter of 5.7 cm (2 1/4 in.) at dE/dt = 5 joules/nanosec.

$$\begin{array}{lcl} \text{spall ring diameter} & = & 1.5 + 0.84 \text{ dE/dt} \\ \text{(cm)} & & \text{(joules/nanosec)} \end{array}$$

For further increase in dE/dt, the diameter remains constant at 5.7 cm.

4.1.2 Targets with BHN of 100. When we change from the harder armor to armor with BHN of 100, we have a distinct increase in spall ring diameter. Figure 4 shows this increase. The plotted points are the BHN 100 data, and the curve is that of the harder armor of Figure 3.

4.1.3 "Super Spall."

Figure 3 suggests a division of the data into two parts: dE/dt < 5 joules/nanosec with varying spall ring diameter; dE/dt > 5 joules/nanosec with constant (maximum) spall ring diameter. Nearly the same partitioning of the rounds occurred in Reference 2 where debris measurements were characterized. In that report the rounds were separated by a critical target thickness, eight centimeters. The data support this value only approximately. A critical target thickness of 7.5 cm would produce a partitioning of the rounds identical to that provided here by a critical dE/dt of 5 joules/nanosec.

Reference 1 refers to the spall of the thinner targets as "super spall," a label coined at BRL to identify this large-diameter,

*Strictly speaking we cannot equate the termination of penetration to a zero rate of energy transfer. Penetration into infinitely thick steel targets actually ceases when the penetration velocity decreases to 0.1 cm/microsec.⁵ In this experiment all targets were sufficiently thin to permit perforation. The lowest value for our rate of energy transfer parameter, 0.28 joules/nanosec, occurred for a 30.5 cm thick target at two cone diameters standoff. A target about ten centimeters thicker would prevent perforation. In that case our rate of energy transfer parameter would be 0.09 joules/nanosec rather than 0.

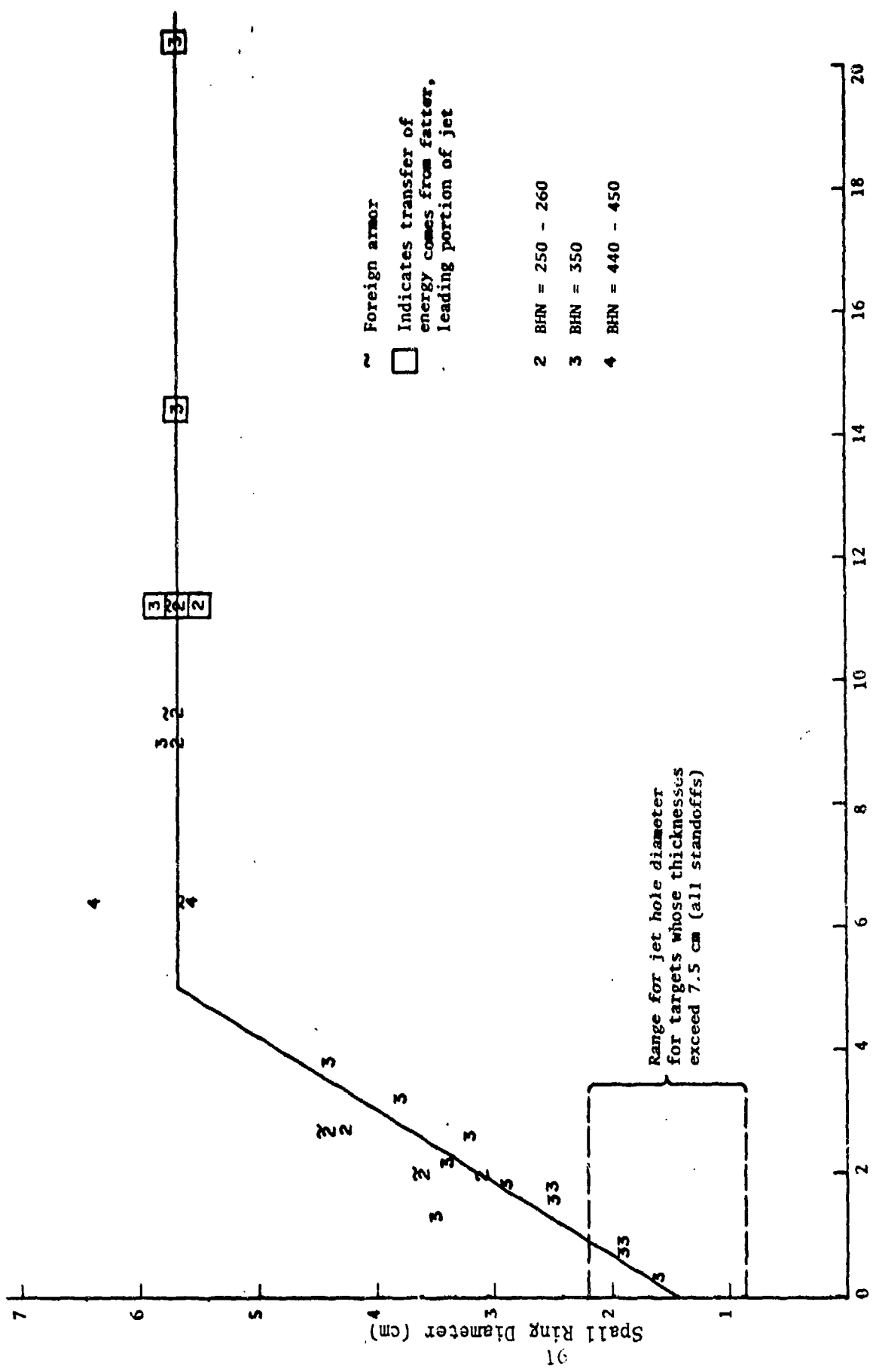


Figure 3. Spall Ring Diameter vs Rate of Energy Transfer at One cm Before Surface of Armor Plate with BHN from 250 to 450

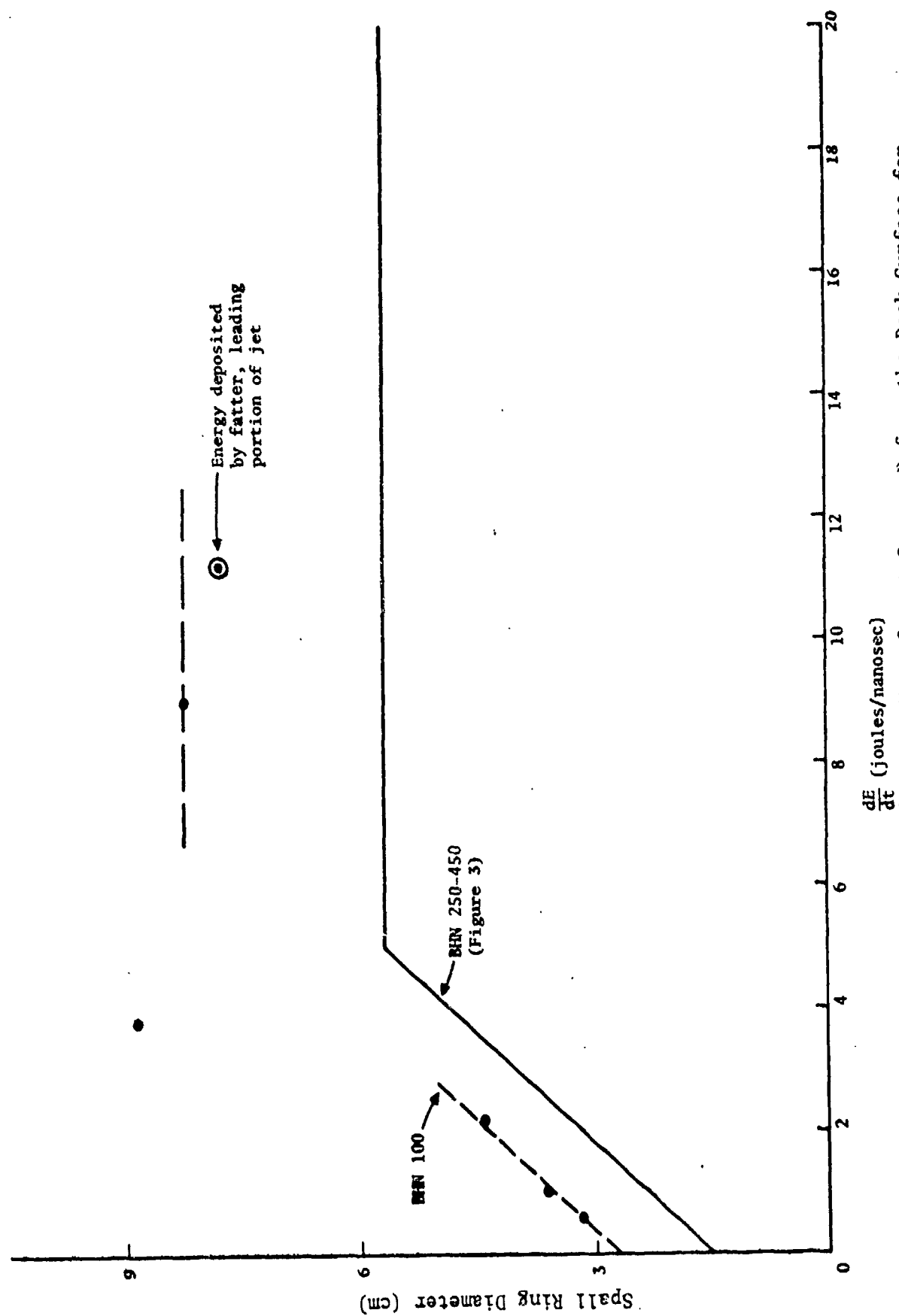


Figure 4. Spall Ring Diameter vs Rate of Energy Transfer at One cm Before the Back Surface for Armor Plate of BHN 100

donut-shaped, spall scab which fragments into large pieces. In view of Figure 3 we feel this super spall ring to be of fixed diameter, 5.7 cm. From References 1 and 2 we learn that the weight of this ring increases with increasing dE/dt . We conclude that the thickness of the super spall scab, and not its diameter, increases with increasing dE/dt .

Because of the existence of super spall, let us put aside temporarily our dE/dt parameter and examine the primary jet characteristics involved. As stated earlier, the leading portion of the jet has about twice the diameter of the remainder of the jet breakup. The leading portion, therefore, can be solely responsible for as much as the initial 3.4 cm of penetration. For thin targets, then, the spall effect is dominated by the fatter, leading portion of the jet. This fatness of the leading portion magnifies dE/dt by a factor of four over the trailing portion of the jet. The questions arise: Does super spall result from thin targets per se or from the nearness of the fatter portion to the back surface of the plate? Would a jet, deprived of its leading portion, produce super spall from thin plates?

4.2 Peripheral Spall Trajectories

Having determined the diameter of the spall scab, that is, the ring of incipient spall, we also want to know the direction, speed, and size of the spall fragments emanating from this ring. The speed and size have been characterized in Reference 1. That report also estimated the direction by postulating that all particles, spall and ejecta, traveled along concurrent straight line paths, these lines meeting at a point five centimeters ahead of back surface of the plate and lying on the jet axis (normal impact). Presumably this point was selected after scanning all debris data. Here we will look only at the paths of spall particles located at the periphery of the spall scab, and these paths we will define by the angle they make with the jet axis.

To determine the path angle of peripheral spall, visualize a frustum of a right circular cone circumscribing the debris fragments trapped in the collecting medium. The smaller base has a diameter equal to the measured spall scab diameter and is superimposed on the spall scab. We call the semi-vertex angle of this cone the "measured" path angle of peripheral spall. We make the usual assumptions, tacit in Reference 1:

- . Spall particles travel along straight line paths through air and through the collecting medium (no Snell effect).
- . Spall particles fan out with no possibility of collision.

As seen in Table 1, replicate firings were made at all test conditions. Ordinarily one would plot all data points individually or plot

averages of replicated points. In this part of the experiment, unfortunately, bias was introduced by two forms of fragment culling:

- . The debris particles trapped in the first 2.5 cm of the Celotex collection medium were discarded because they were too numerous and, hopefully, of negligible contribution to vulnerability assessment. Consequently, because of the larger path angle it makes, a peripheral spall fragment could be discarded even though it traversed 40 per cent more Celotex than a non-discarded inner-lying debris particle.
- . The test set-up was such that spall particles lying outside of a specified spatial cone were retained only on a few occasions. It was thought that significant fragments would lie only within this cone. The spatial cone is defined² as: (1) axis coinciding with jet axis; (2) vertex 5.08 cm ahead of the back surface of the target plate; and (3) semi-vertex angle of 41.37 degrees. For the data in this report this is equivalent to saying that if the path angle of a peripheral spall particle exceeds 43.5 degrees, it likely was discarded.

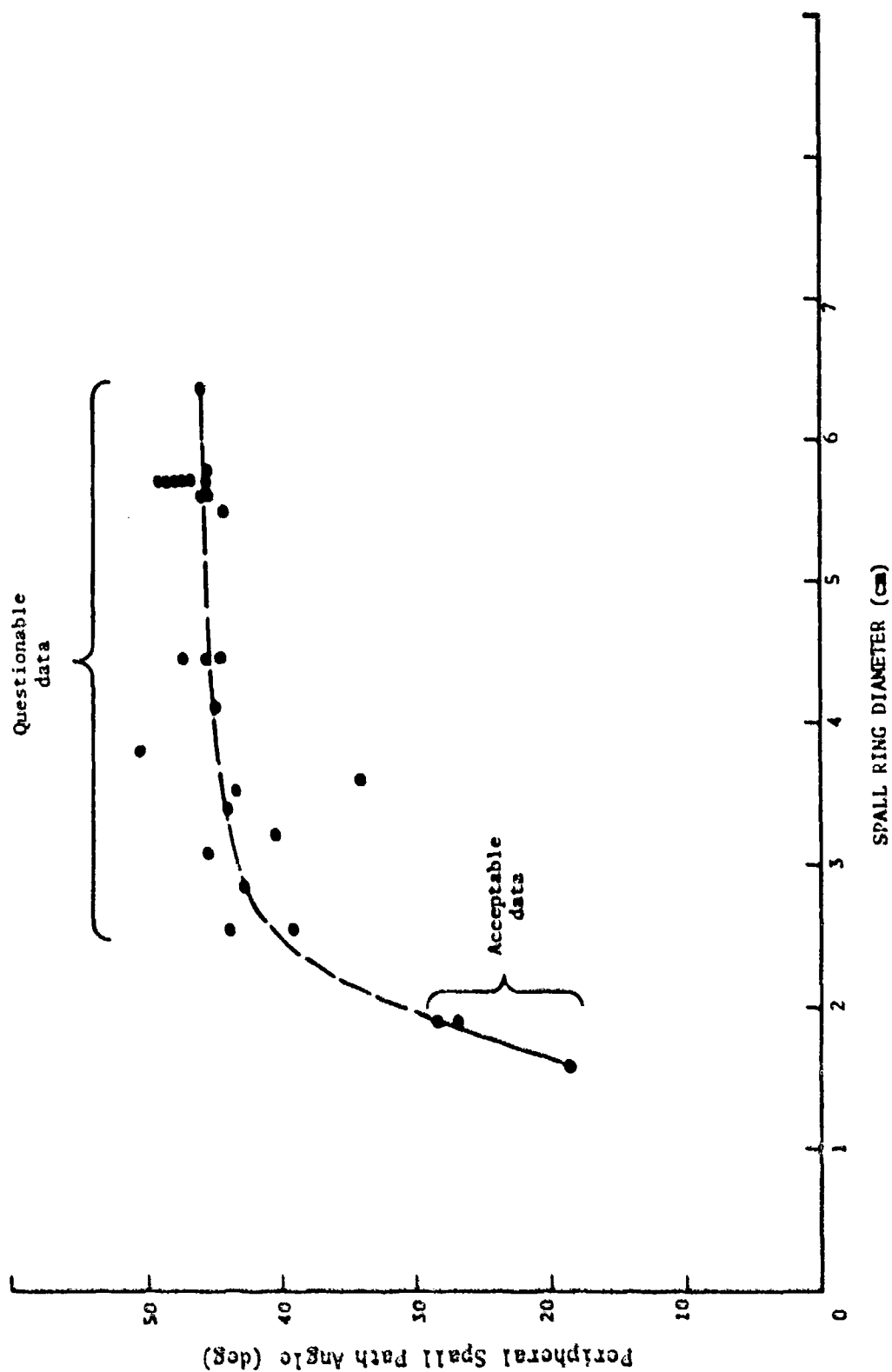
Because of this bias we selected the largest path angle from replicated firings as representative of the test condition.

4.2.1 Target Plates of BHN from 250 to 450. Figure 5 plots the peripheral spall path angle vs spall ring diameter for armor plate with BHN ranging from 250 to 450. We believe the three data points having diameters under two centimeters represent data free from the above bias and are, therefore, acceptable data. These points are the measurements for the thickest target, 30.5 cm, in the experiment. All other data points look suspiciously near the maximum path angle permitted in the collection process.

4.2.2 Target Plates of BHN 100. Figure 6 plots the peripheral spall path angle vs spall ring diameter for target plates of BHN 100. All these data are similarly questionable.

5. CONCLUSIONS

(1) Spall ring diameter correlates well with the rate of energy transfer parameter defined in this report. This empirical information can be incorporated into a hydrocode as part of a recipe for spall release simulation. Information on the thickness of the spall ring is needed.



(Questionable Data)

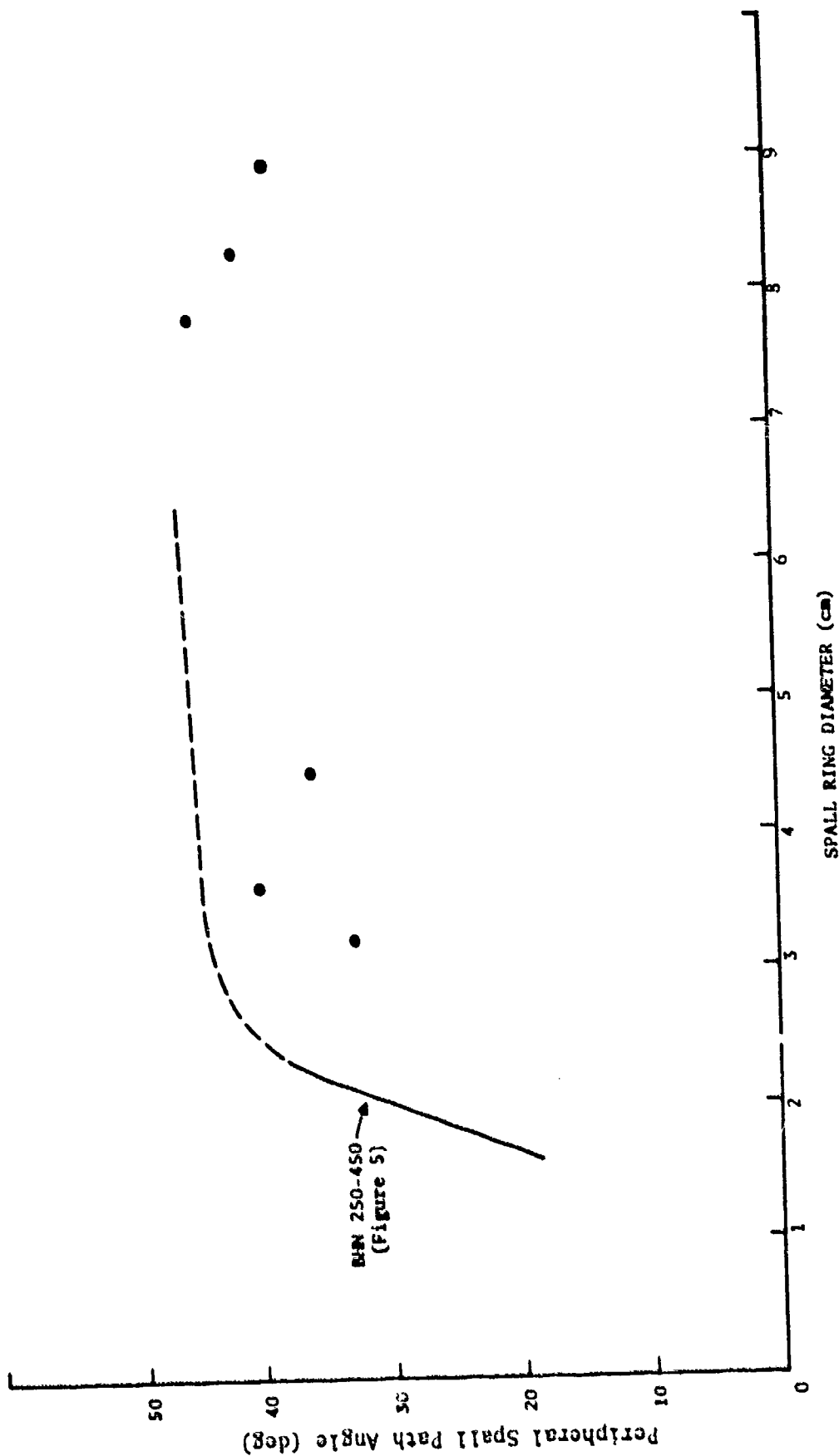


Figure 6. Trajectories of Peripheral Spall Particles vs Spall Ring Diameter for Armor Plate of BHN 100

(2) No effects were observed for variation in target hardness for BHN from 250 to 450. Plates with BHN of 100, however, gave larger spall rings. Also, steel with BHN > 500 may prove sufficiently brittle to alter the spall characteristics drastically.

(3) No effects were observed between foreign and domestic armor.

(4) Super spall may depend upon how near the fatter leading portion of the jet gets to the target's back surface before being totally consumed in the penetration process.

(5) Peripheral spall trajectories are uncertain since the needed data may have been discarded in the experiment.

DISTRIBUTION LIST

<u>No. of Copies</u>	<u>Organization</u>	<u>No. of Copies</u>	<u>Organization</u>
12	Commander Defense Documentation Center ATTN: DDC-TCA Cameron Station Alexandria, VA 22314	1	Director US Army Air Mobility Research and Development Laboratory Ames Research Center Moffett Field, CA 94035
1	Director Defense Advanced Research Projects Agency 1400 Wilson Boulevard Arlington, VA 22209	1	Commander US Army Electronics Command ATTN: DRSEL-RD Fort Monmouth, NJ 07703
1	Director for Planning and Evaluation Office of the Secretary of Defense Washington, DC 20301	1	Commander US Army Missile Research and Development Command ATTN: DRDMI-R Redstone Arsenal, AL 35809
1	Commander US Army Materiel Development and Readiness Command ATTN: DRCDMA-ST 5001 Eisenhower Avenue Alexandria, VA 22333	1	Commander US Army Tank Automotive Development Command ATTN: DRDTA-RWL Warren, MI 48090
1	Commander US Army Materiel Development and Readiness Command ATTN: DRCPM 5001 Eisenhower Avenue Alexandria, VA 22333	2	Commander US Army Mobility Equipment Research & Development Cmd ATTN: Tech Docu Cen, Bldg 315 DRSME-RZT Fort Belvoir, VA 22060
1	Commander US Army Materiel Development and Readiness Command ATTN: DRCCP 5001 Eisenhower Avenue Alexandria, VA 22333	1	Commander US Army Armament Materiel Readiness Command Rock Island, IL 61202
1	Commander US Army Aviation Research and Development Command ATTN: DRSAB-E 12th and Spruce Streets St. Louis, MO 63160	1	Commander US Army Armament Research and Development Command Dover, NJ 07801
		1	Commander US Army Frankford Arsenal ATTN: SARFA-L7000, Mr. Marcus Philadelphia, PA 19137

DISTRIBUTION LIST

<u>No. of Copies</u>	<u>Organization</u>	<u>No. of Copies</u>	<u>Organization</u>
1	President US Army Aviation Test Board Fort Rucker, AL 36360	1	Director US Army TRADOC Systems Analysis Activity ATTN: ATAA-SL (Tech Lib) White Sands Missile Range NM 88002
1	President US Army Infantry Board Fort Benning, GA 31905	1	Commander US Army Experimentation Command Fort Ord, CA 93941
1	Commander US Army Harry Diamond Labs ATTN: DRXDO-TI 2800 Powder Mill Road Adelphi, MD 20783	1	Commander US Army Armor School ATTN: Armor Agency Fort Knox, KY 40121
4	Director US Army Materials and Mechanics Research Center ATTN: DRXMR-ATL Mr. Frank McElaney Mr. J. J. O'Connor Mr. E. F. Joyce Watertown, MA 02172	1	HQDA (DAMA-ARD) Washington, DC 20310
1	Commander US Army Natick Research and Development Command ATTN: DRXRE, Dr. D. Sieling Natick, MA 01762	1	HQDA (DAMA-DDA) Washington, DC 20310
1	Commander US Army Foreign Science and Technology Center ATTN: DRXST-CB, Mr. Petrie Federal Office Building 220 Seventh Street, NE Charlottesville, VA 22901	1	Chief, US Army Concepts Analysis Agency ATTN: STAG-SM 8120 Woodmont Avenue Bethesda, MD 20014
1	Commander US Army Training and Doctrine Command ATTN: ATCD-CS-M-AR Fort Monroe, VA 23551	1	Commandant US Army Command and General Staff College ATTN: Archives Fort Leavenworth, KS 66027
		2	Chief of Naval Operations Department of the Navy ATTN: OP-05 OP-34 Washington, DC 20350
		3	Commander US Naval Ordnance Systems Cnd ATTN: ORD-0632 ORD-035 ORD-5524 Washington, DC 20360

DISTRIBUTION LIST

<u>No. of</u> <u>Copies</u>	<u>Organization</u>	<u>No. of</u> <u>Copies</u>	<u>Organization</u>
2	Commander US Naval Surface Weapons Ctr ATTN: Code KEC Code DG-10 Dahlgren, VA 22448	1	AFATL (DLJM, Mr. Dittrich) Eglin AFB, FL 32542
2	Commander US Naval Weapons Center ATTN: Code 753 Code 40701, Mr. Keith China Lake, CA 93555	1	AFFDL (Dr. F.J. Janik, Jr.) Wright-Patterson AFB, OH 45433
1	Commander US Naval Ammunition Depot ATTN: RD-3 Crane, IN 47522	1	Director Energy Research and Development Administration Los Alamos, NM 87115
1	Commandant US Marine Corps ATTN: Code AAP Washington, DC 20380	1	Thor Group Falcon R&D Company ATTN: Mr. R. J. Pipino 696 Fairmont Avenue Baltimore, MD 21204
1	Director Development Center MCDEC Quantico, VA 22134	2	Systems, Science & Software ATTN: R. T. Sedgwick P. L. Anderson P. O. Box 1620 La Jolla, CA 92037
1	HQ USAF (Jack Martin) Room 4E968, The Pentagon Washington, DC 20330	2	Southwest Research Institute ATTN: Mr. Alex Wenzel Dr. Wilfred Baker 8500 Culebra Road San Antonio, TX 78284
1	HQ USAF (AFSA) Washington, DC 20330		<u>Aberdeen Proving Ground</u> Marine Corps Ln Ofc Dir, USAMSAA ATTN: B. Oehrli J. Sperrazza Gerard Johnson Cdr, USATECOM